International Journal of Geographical Information Science
Vol. 21, No. 1, January 2007, 1–20

Taylor & Francis
Taylor & Francis Group

Research Article

Modelling and prediction of GPS availability with digital photogrammetry and LiDAR

GEORGE TAYLOR*†, JING LI†, DAVID KIDNER†, CHRIS BRUNSDON‡ and MARK WARE†

†GIS Research Centre, School of Computing, University of Glamorgan, CF37 1DL, Wales

‡Department of Geography, University of Leicester, London Road, Leicester LE1 7RU, England

(*Received 1 February 2006; in final form 25 April 2006*)

This paper describes an automated method for predicting the number of satellites visible to a GPS receiver, at any point on the Earth's surface at any time. Intervisibility analysis between a GPS receiver and each potentially visible GPS satellite is performed using a number of different surface models and satellite orbit calculations. The developed software can work with various ephemeris data, and will compute satellite visibility in real time. Real-time satellite availability prediction is very useful for mobile applications such as in-car navigation systems, personal navigations systems and LBS. The implementation of the method is described and the results are reported.

Keywords: GPS; DSMs; Photogrammetry; LiDAR; Line Of Sight (LOS)

1. Introduction

The use of Global Navigation Satellite Systems (GNSS), such as the United States' Global Positioning System (GPS), GLONASS the Russian equivalent and the proposed European Galileo system, on the surface of the Earth, may be severely compromised by limited satellite visibility and unwanted reflections of the signals (multipath). Multipath is a problem that is not addressed by this paper; however, it is the focus of current work. If insufficient satellites (normally fewer than four) are visible, a 3D location cannot be computed. Hence, there is a requirement to test for continuity, reliability and accuracy of GNSS to provide positioning information, at various times and places. This is especially true for many transportation applications such as land surveying, fleet management, speed limitation, and vehicle navigation. Although many GPS manufacturers supply project-planning packages as part of their receiver systems, all assume a locally flat Earth where simple elevation masks can be manually added for individual obstructions around a point location. These packages are useful but restricted to static point positioning applications with limited, unrealistic obstructions, and more

little or no use as a test bed for transport applications of GNSS, because in these cases the nature and distribution of obstructions are changing constantly.

Over the last decade, with the increased availability of high-resolution laser scanning surface models and technological advances in digital photogrammetry, the accuracy of GPS satellite availability prediction has been improved dramatically through tight integration with digital surface models, especially in urban areas. The limitations, such as the lack of terrain information in the traditional GPS mission planning software, is a limitation to accuracy, efficiency and productivity for the surveyor. A number of researchers have proposed methods to address this issue. Boulianne *et al.* (1996) suggested a new photogrammetric method of generating obstruction diagrams based on floating cones injected into the stereo model, to reduce the amount of work in field and photogrammetric survey. Similarly, Walker and Sang (1997) used the elevation mask angles that were derived from a photogrammetrically-created digital terrain model. The conclusion drawn in their work is that accurate DTM information is invaluable to the users of high precision RTK (i.e. Real Time Kinematic) GPS in harsh environments. Moreover, in recent years, LiDAR (light detection and ranging) has become more accessible than ever to the GIS community. Its high resolution and accuracy is well-suited for satellite visibility modelling. Verbree *et al.* (2004) reconstructed building models from LiDAR point clouds with the aid of ground plan maps. The building polygons were split into segments such that the LiDAR point cloud within each segment can be represented by predefined roof structures, such as a flat roof, gable roof or hip roof. The reconstructed building model was then used to predict the signal coverage of GPS/Galileo in a dense built-up area in Delft, The Netherlands. The simulation results for the 50 observer points show that the availability of the GPS and Galileo is nearly 100% (i.e. no less than four satellites in view). However, the result was not verified with real observations. In addition, a concern is that fitting LiDAR points into segmented ground plans for rooftop reconstruction may have a bearing on the prediction accuracy. In fact, in terms of a real-time simulation of GPS availability, a number of technical issues including coordinate transformation of satellite positions from WGS84 to a local datum or vice versa, the use of a range of ephemeris (e.g. almanac, broadcast and precise ephemeris), the choice of terrain data, line of sight analysis in a GIS and the validation and verification of the prediction results should be addressed.

The work described in this paper aims to identify the accuracy and complexity of 3D digital feature and terrain models required for GPS availability modelling. Furthermore, a real-time GPS mission planning package based on ESRI's ArcGIS9 has been developed to simulate satellite availability as a vehicle travels along the road in urban areas (see figure 3). For example, a specific bus route at specific times of the day can quickly be analysed to determine if GPS is a feasible option for an arrival/schedule information system. A variety of line of sight (LOS), terrain modelling and coordinate transformation techniques are presented in detail in the following sections.

from WGS84 to OSGB36 prior to Line of Sight (LOS) analysis in a GIS. In general, transformation between different 3D Cartesian coordinate systems can be computed through the well-known 3D conformal transformation (i.e. three rotation parameters, three translation parameters and one scale factor). In order to achieve a better accuracy, the National Grid Transformation and Geoid Model OSTN02/OSGM02 were used to convert WGS84 3D Cartesian coordinates to easting, northing and orthometric height (i.e. the height above mean sea level) and vice versa.

As stated by the Ordnance Survey, the horizontal transformation accuracy has been improved from 0.2 m to 0.1 m RMS and the vertical accuracy has been improved from 0.05 m to 0.02 m RMS compared to the previous models OSTN97/OSGM91 (Ordnance Survey 2004). For real-time simulation, the coordinate transformation was computed on the fly and embedded into the developed mission planning software package. However, a problem remains in that the OSTN02/OSGM02 does not function with the WGS84 coordinates of the satellites in space, since they are obviously outside the transformation area (i.e. outside the UK). Hence, satellite coordinates have to be first projected along their LOS into the transformation area prior to conversion to the local grid at each epoch (second). Figure 1 shows receiver A, positioned on the ground, and a satellite position B in space. The projected satellite coordinates C along the LOS vector $\overrightarrow{AB}$ can be calculated using equation (1), provided that the length of the vector $\overrightarrow{AC}$ in equation (2) is known and predetermined by a user. A similar approach was taken by Vrhovski (2003).

$$\overrightarrow{OC} = \left(\overrightarrow{OB} - \overrightarrow{OA}\right) \times scalar + \overrightarrow{OA} \tag{1}$$

where

$$scalar = \frac{\left\|\overrightarrow{AC}\right\|}{\left\|\left(\overrightarrow{OB} - \overrightarrow{OA}\right)\right\|} \tag{2}$$

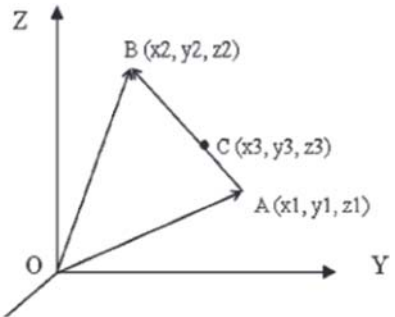

Table 1. Summary of elevation data evaluated in this research.

Product	Abbreviation	Horizontal resolution (m)	Vertical accuracy (m) RMSE	Format
LiDAR DSM first pulse return (InfoTerra)	1 m LiDAR DSM FP	1	±0.15	Points
LiDAR DTM last pulse return (InfoTerra)	1 m LiDAR DTM LP	1	±0.15	Raster
Airborne IFSAR DSM (NextMap Britain)	5 m RADAR DSM	5	±1	Raster

Note that, intuitively, the closer the objects are, the more likely they are to produce obstructions. However, care has to be taken when choosing the predetermined length of the vector $\overrightarrow{AC}$, as features on the surface model that block the LOS between observers and satellites could be bypassed if the length of the vector $\overrightarrow{AC}$ is too short (e.g. a distant hill). The length of vector AC is calculated such that the scaled satellite positions are located outside the horizontal boundary of the test area. As a result, all modelled potential obstructions in the DSM are considered in the LOS analysis.

2.2 *Height data*

As mentioned earlier, one of the objectives of this research is to investigate the accuracy and complexity of 3D digital surface models required for GPS availability modelling. A range of height data and 2D plan maps were used and evaluated with respect to the prediction accuracy. Table 1 shows a summary of the height data used in this research.

It can be seen clearly from figure 2 that far more fine detail can be picked out with 1m LiDAR when compared with 5 m radar data.

In addition to the height data, 2D building polygons of the testing area, derived from Ordnance Survey Master Map, were incorporated into the LiDAR data to enhance the performance of visualization and LOS analysis. The positional error of OS Master Map at 1:1250 scale is less than $\pm 1.1m$ at 99% confidence level (Ordnance Survey 2005).

2.3 *Digital photogrammetry and LiDAR*

Photogrammetry is a traditional technique for measuring 3D coordinates of objects from a pair of overlapping photographs. In recent years, the rapid development of digital photogrammetry (i.e. softcopy photogrammetry) has led to increased productivity of generating topographic maps and digital elevation models (DEMs). However, LiDAR is now often preferred to this traditional terrain data acquisition technique due to the fact that LiDAR can offer higher productivity, higher resolution and superior accuracy.

At present, 1 m spacing LiDAR data have been made readily available to

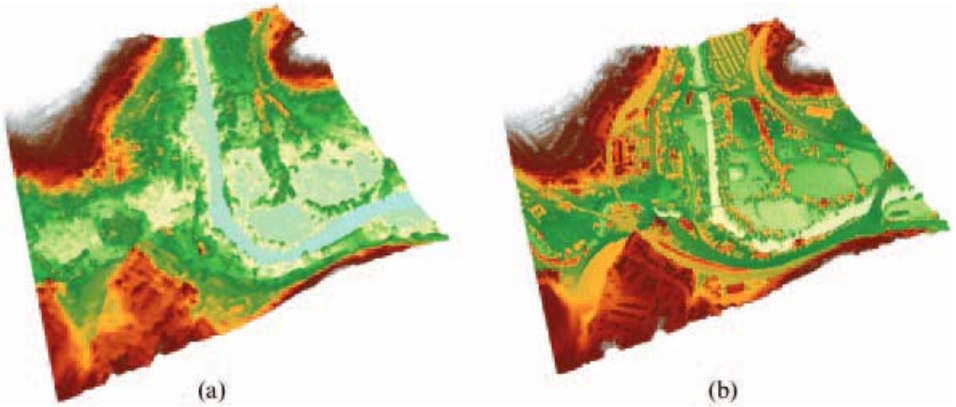

Figure 2. (a) 5 m Radar DSM; (b) 1 m LiDAR DSM FP.

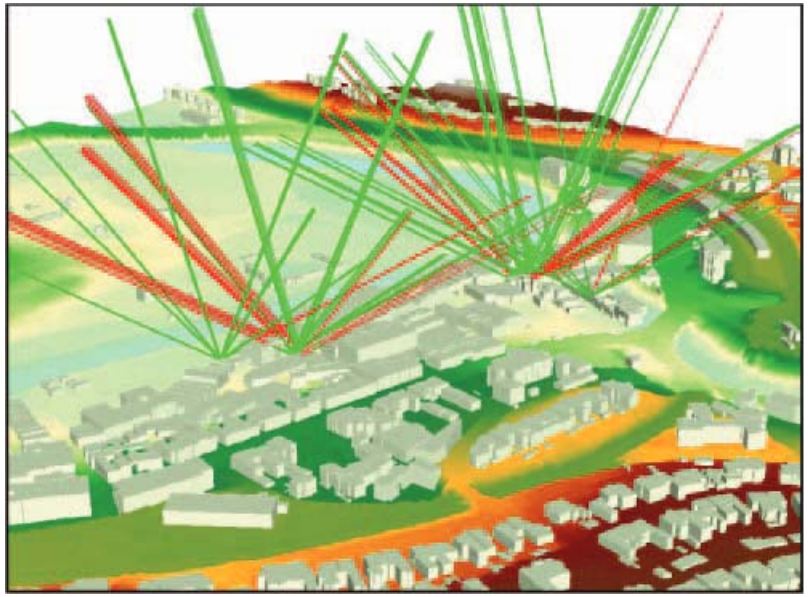

Figure 3. LOS to GPS satellites.

For this experiment, a state-of-the-art photogrammetric system from Z/I Imaging was used to measure all the building roofs in 3D stereo from scanned aerial photographs. The photos used here have 25 cm ground resolution and pixel size is 20 microns. Having performed interior, relative and absolute orientations, the summary statistics page, figure 4, shows a variety of parameters to indicate the quality of the model. Note that the sigma value on the top right corner is the computed standard deviation in the least squares adjustment. It is the single most important statistic for overall analysis of the results. As a rule of thumb, for a 20

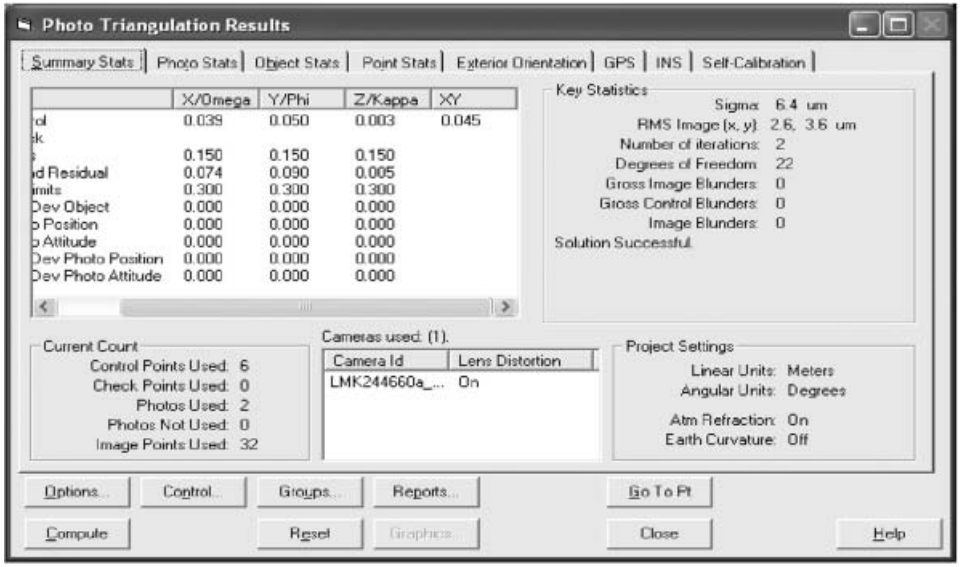

Figure 4. Summary statistics page.

used in the project. Theoretically, a minimum of about two horizontal and three vertical ground-surveyed photo control points should be used per stereo model. However, redundant control points may lead to higher accuracy and better averaging in the least squares adjustment. Six 3D control points were collected by dual frequency phase static GPS, and their configuration is shown in figure 5.

Figure 6 shows the fit to control points. The combined 3D ground residual errors (V(XYZ)), which are the differences between the computed control point coordinates and the measured ones, are all less than 10 cm. Thus, a satisfactory solution is achieved.

2.4 *Digital surface modelling and LOS analysis*

In order to perform LOS analysis with the raw LiDAR points (i.e. the first row in table 1), points data can be either interpolated into a raster grid or triangulated into a triangulated irregular network (TIN) using the interpolation algorithm or Delaunay triangulation provided by ArcGIS9 3D Analyst. It should be noted that the effect of the interpolation algorithm and various LOS algorithms based on TIN and Grid have been extensively researched over the last ten years (see Kidner (2003) and Dorey (2002) for a thorough investigation of this issue). The interest here is particularly focused on how the integration of LiDAR and digital photogrammetry affects LOS results in real-time simulation of GPS availability. Having carefully examined both the TIN and raster surface models created from the raw LiDAR points, the inaccuracies in building representation, such as sloping walls and erroneous triangles on rooftops that fail to represent the true shape of roof

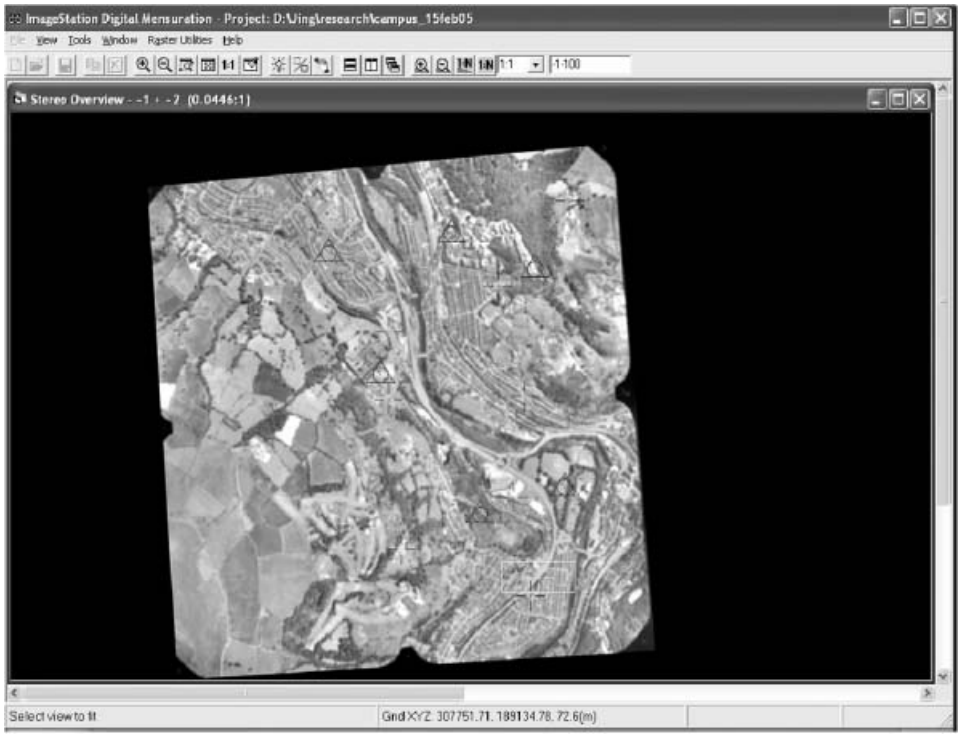

Figure 5. Six control points used in the project.

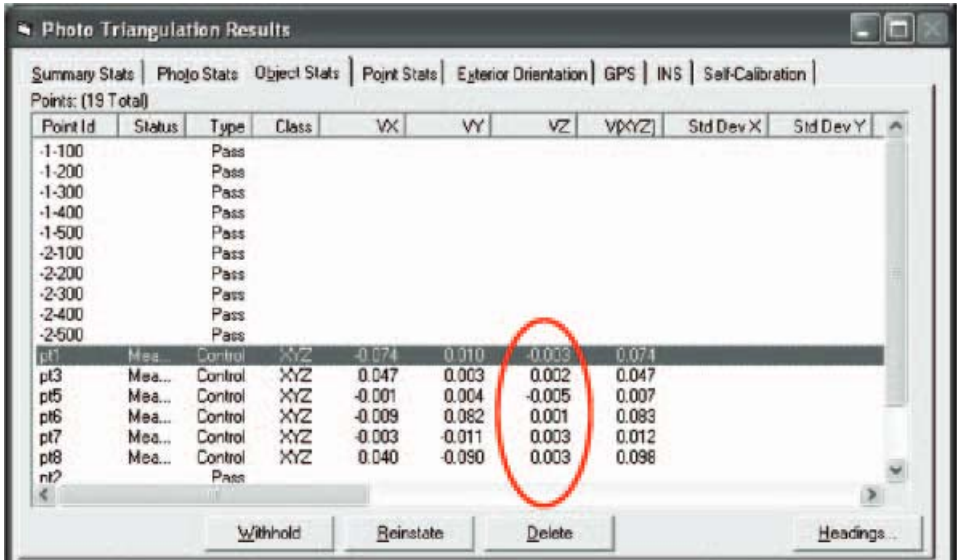

model accurately sharp surface discontinuities like break-lines (Thompson and Maune (2001)). In this case, supplementary information from other sources such as 3D break-lines compiled photogrammetrically can be incorporated into the LiDAR data by using constrained Delaunay triangulation. The steps taken to combine photogrammetry with LiDAR are explained as follows:

1. The height of the building foundation is computed by taking the average of all the bare-Earth LiDAR points that fall into each building footprint.
2. The height computed from Step 1 is assigned to each photogrammetrically-created building footprint.
3. Clean up the LiDAR DSM FP points (see table 1) that fall inside the building footprints.
4. Add the building footprints to the LiDAR DSM FP data to create flat building foundations. The heights associated with the building footprints are computed in Steps 1 and 2.
5. 1 cm buffers are created, which encompass the original building footprints in order to create near-vertical walls. This is because a conventional TIN model is 2.5D, which means that two different heights are not allowed at the same X, Y position.
6. Add the photogrammetrically-created rooflines to the model computed in Step 5 through constrained Delaunay triangulation, which guarantees that no triangles can cross the rooflines.

The resulting model from the above procedure is shown in figure 7.

Figure 8 shows the near-vertical walls and roof structures, which look more realistic than the original LiDAR data. The 3D line work is collected in MicroStation and stored in a computer-aided design (CAD) design file (i.e. a DGN file).

It should be noted that the above-mentioned approach has its limitations. For example, too many vertices are added to the building edges to enforce near-vertical walls. It is also difficult to model complex man-made objects like holes and bridges without a true 3D data structure. Tse and Gold (2003) extended the TIN to represent tunnels and bridges by introducing a subset of CAD-type Euler operators in conjunction with a Quad-Edge data structure. For this experiment, the accuracy is the major concern, thus the simple constrained Delaunay triangulation sufficed.

In terms of satellite visibility analysis, the sensitivity of LOS to GPS satellites was found to be very high. For example, a person turning around on a spot will gain and lose satellites. Therefore, it is beneficial to add building polygons to LiDAR data for visual inspection of LOS results as shown in figure 3, where a green LOS vector indicates a satellite is visible. In figure 3, building polygons were extruded using the estimated height from 1 m LiDAR DSM FP (see table 1). The resulting extruded buildings were then put back onto the 1 m LiDAR DTM LP (i.e. the bare-Earth model) to form a single surface model. The LOS algorithm was modified accordingly.

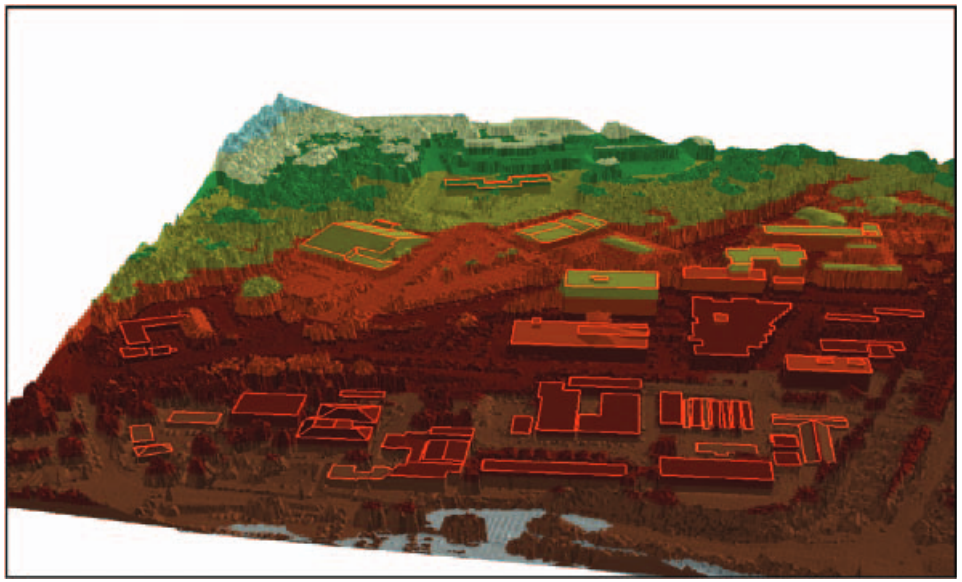

Figure 7. TIN created from photogrammetry and LiDAR.

to be blocked. This approach may be extended to work with other 3D vector data formats such as CAD data.

3. Field test and results

Two field tests were conducted to evaluate the LOS results on a variety of digital surface models. The first test aims to test a large number of Differential GPS points (DGPS) in a dynamic mode. The second test puts more emphasis on photogrammetrically created buildings for comparison with LiDAR DSM FP in terms of LOS accuracy.

3.1 *Test 1*

To test the accuracy of the developed mission planning package, GPS Coarse Acquisition (C/A) code observation data were collected using Leica 500 series geodetic GPS receivers in a dense built-up area near the University of Glamorgan in Wales (figure 9). Simultaneously, a GPS base station was set up on the roof of the School of Computing to record base station data. Unfortunately, the Real Time Kinematic (RTK) data were not available due to the poor coverage of the GPS signal in the testing area, which has very narrow streets with tall buildings on either side.

All available satellites visible to both receivers were used in the position solution computation. The number available varied throughout the route from none to eight. DGPS were computed and are assumed to be the truth. It can be argued that the more accurate RTK positions should be used. However, at this initial stage of the experiment, it is interesting to see how the performance of the real-time simulation varies with inaccuracies in DGPS positions. There were a total of 767 DGPS points available throughout the route. Results are given in table 2.

3.2 *Test 2*

In order to test how differently the LiDAR and photogrammetry models perform in terms of LOS analysis, 20 high-accuracy kinematic GPS points were collected on the campus, placing greater emphasis on photogrammetrically created building polygons (figure 10). The results are shown in table 3.

4. The analysis of the results

In test 1, table 2 shows that 1 m LiDAR data is significantly better than 5 m radar by almost 890 satellites modelled correctly out of 5889 satellites. Therefore, low-resolution DSMs should not be used in GPS mission planning especially in dense built-up areas, since buildings close to the receiver are not adequately modelled. The prediction accuracy of LiDAR data is quite satisfactory, although errors exist. In

Figure 9. All GPS positions used in test 1.

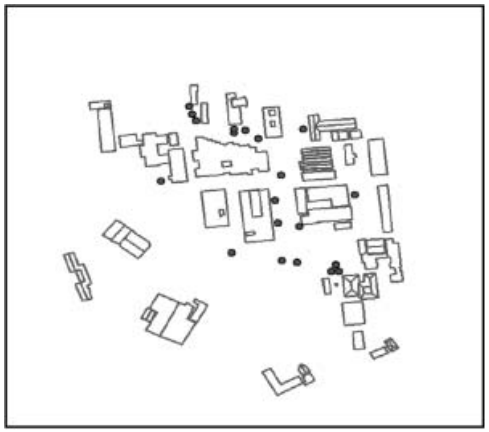

Figure 10. Twenty kinematic GPS points.

Table 3. Results for 20 kinematic points.

Type of DSMs	Number of satellites modelled correctly
5 m radar DSM	63/160 satellites (39%)
1 m LiDAR DSM FP	145/160 satellites (90%)
1 m LiDAR + photogrammetry	144/160 satellites (90%)

fact, a perfect representation of urban areas is not possible, as the errors caused by the laser instrument, GPS/INS and coordinate transformation all propagate through into the final LOS results. Test 1 also proved that real-time satellite availability modelling can be done with a large number of known observation points over a very short time interval.

Test 2 aims to reveal how the two surveying techniques affect the LOS results differently. As shown in table 3, the simulated number of satellites matches up quite closely with that of the observed satellites. It can be seen that there is one satellite difference between photogrammetry and LiDAR.

Having carefully examined this one satellite difference visually, it was seen that the building eaves measured by photogrammetry were responsible for blocking the LOS (see figure 11). This can be explained by the fact that, for that particular building, the building eaves are overhanging by almost one metre and as such the building footprints cannot be seen on the stereo model; this causes the error in the LOS analysis. In practice, for mapping users, building eaves are usually classified as building footprints.

Apart from this artifact, the photogrammetric model lines up with the original LiDAR model quite closely in a vertical range of 10 cm, which indicates that both LiDAR and photogrammetry can offer a very high accuracy. However, digital photogrammetry is less productive than LiDAR due to the time and effort involved at the terrain data acquisition stage; this is especially true for very large areas or where the heights of terrain features vary over a wide range (the automatic elevation collection tool may not perform well in these areas, meaning that significant manual editing is required to capture the 3D break lines).

5. Viewshed analysis

The purpose of creating a viewshed for the satellites above a particular elevation mask angle at a specific time is to assist in GPS mission planning for a very large area. For example, a mission planning scenario might require an answer to the question: 'Is GPS a viable solution for a bus schedule and arrival information system in London?'

Viewsheds may be created from grid-based or TIN models of the terrain. For this project, a grid-based model is used, as grids lend themselves to particularly simple methods of deriving the viewshed, although they are limited by the resolution of the grid itself (Jones 1997). It is quite obvious from studying figures 12 and 13 that the viewshed computed from 1 m LiDAR is far more accurate and detailed than that of 5 m radar DSM. In figure 12 the areas highlighted in black indicate areas with less

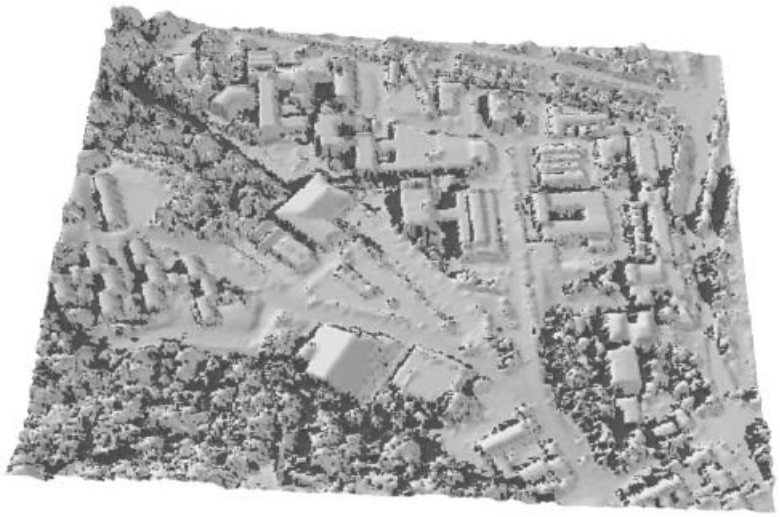

Figure 12. Viewshed computed from 1 m LiDAR DSM.

Furthermore, it should be noted that, although a minimum of four satellites are required to obtain a 3D position, the quality of the position may not necessarily be good due to the possible multipath effect and poor satellite geometry (i.e. high PDOP values). Therefore, a variety of dilutions of precision (DOP) values should also be computed in conjunction with the viewshed.

6. Modelling uncertainty in LOS analysis using Monte Carlo method

As presented in the previous sections, LiDAR provided the most reliable results for the prediction of satellite visibility. It is obvious that, even with the most accurate

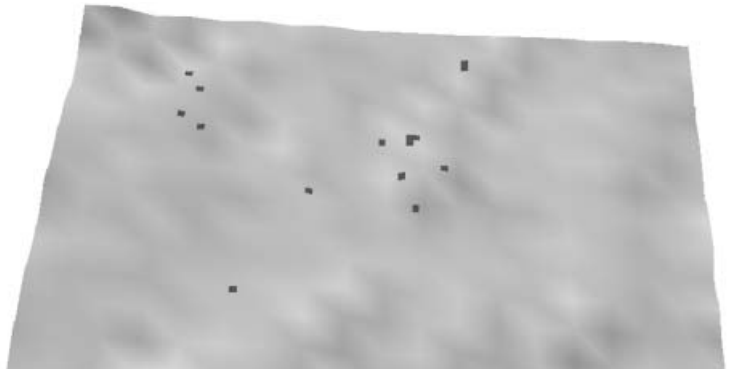

LiDAR data, there has to be some degree of uncertainty in the LOS due to the various error sources (e.g. GPS/INS error in a typical LiDAR system, inaccuracies in satellite and receiver positions). Hence, the above mentioned prediction results need not only to be presented but explained.

To understand the results produced by LiDAR, Monte Carlo simulation (Gentle 2003) is used to model sensitivity of LOS with respect to the terrain. 787 high-precision GPS points were collected on the campus of the University of Glamorgan at 10 s intervals (i.e. approximately 2 h of observations) in order to generate the simulation results for further analysis.

As illustrated in figure 14, three Gaussian random number generators are used to alter the X, Y and Z components of each observed receiver position to generate a further one thousand perturbed receiver positions that are randomly distributed with a zero mean and a standard deviation of 50 cm. Subsequently, the LOS calculation is performed between each perturbed point and the satellites to compute the sensitivity. The sensitivity can be described as the likelihood of a change in the LOS. Note that the interests here only focus on the satellites modelled as visible by the surface model that are actually blocked in reality. In other words, those receiver positions modelled as invisible by the surface model to the satellites are excluded from the experiment. For example, a sensitivity value of 80% means 800 perturbed points out of 1000 are modelled incorrectly as invisible to the satellites.

Furthermore, the shortest perpendicular distance from the LOS vector to the terrain, which is termed Dmin (see figure 14), is also computed to indicate the relationship between the Monte Carlo simulation results and the terrain. It should be noted that Dmin has proven to be a very important indicator to explain why an error in satellite visibility prediction could occur. This will be further explained in the next section.

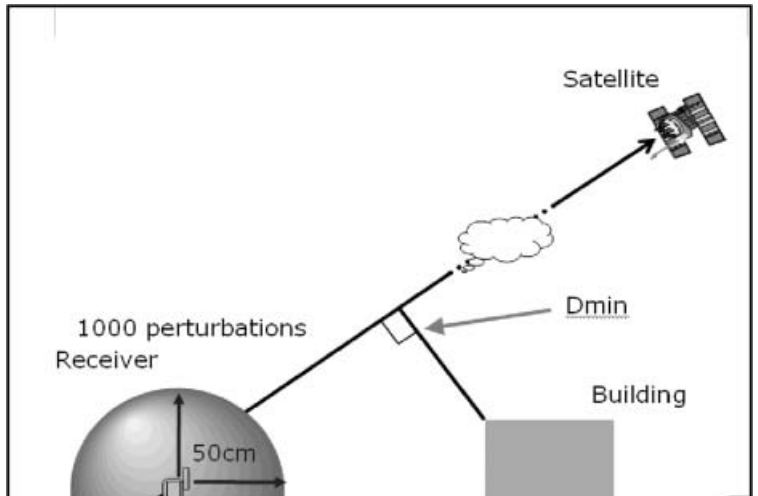

Figures 15 and 16 show the sensitivity plotted against the shortest perpendicular distance (i.e. Dmin) computed from two sets of observations (i.e. 787 points in total). It can be clearly seen from figure 15 that all the prediction errors in the LOS occurred when Dmin is smaller than 2 m. No errors occurred when Dmin is greater than 2 m. Therefore, the conclusion is that the smaller the value of Dmin, the more likely is a LOS prediction error. However, there is a mixture of correct and incorrect predictions shown in figure 15 before 2 m, although incorrect predictions outnumber the correct ones in this experiment. In addition, it seems that 2 m is a critical distance for an error to occur in LOS. Table 4 shows the potential error sources and their magnitudes, though this 2 m threshold is obtained through experiment. However, it should be noted that any obstacles close enough to the LOS may cause a signal strength loss considerably in excess of the free space loss (i.e. Dmin is small enough), even though the LOS path is not actually blocked. This effect is known as diffraction loss, and may have an influence on the LOS prediction error (Parsons 2000).

Figures 15 and 16 also reveal that the sensitivity of the LOS analysis is inversely proportional to the shortest perpendicular distance from LOS to terrain (Dmin)

7. Predicting the probability of computing a 3D position (four or more visible satellites)

One of the most useful outcomes of this experiment is the probability of four satellites being visible at a particular time. The objective here is to compute a viewshed indicating the probability of at least four visible satellites in urban areas.

Since the outcome of this experiment takes one of two values, either 'Correct' or 'Incorrect', a logistic regression model (see for example Hosmer and Lemeshow (1989) or Chambers and Hastie (1992)) is appropriate to calculate the probability of

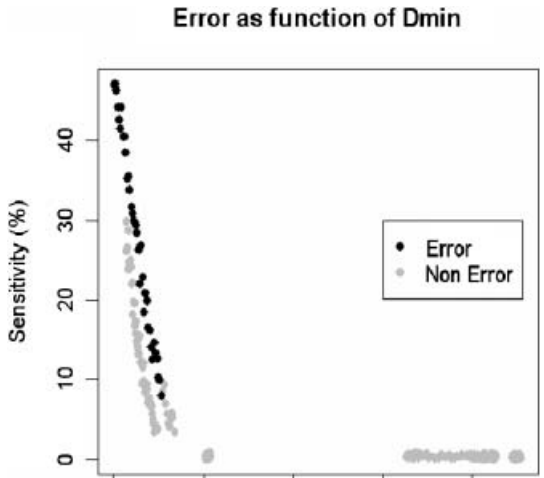

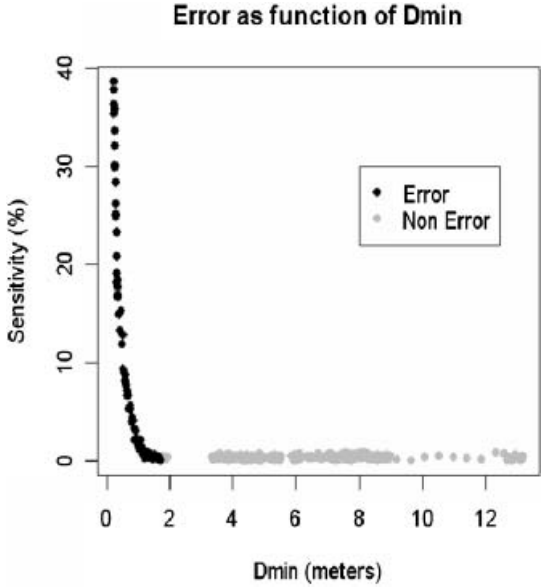

Figure 16. A plot of test 2.

an incorrect LOS prediction for each satellite. A model of this type returns the probability of a 'Correct' value. Thus, unlike ordinary regression models, the output here is restricted to the range [0,1]. In the standard logistic model, if p_i is the probability of a 'Correct' classification for observation i, and the predictor variables are x_{ij} then

$$\frac{e^{p_i}}{1+e^{p_i}} = a_0 + \sum_{j=1,m} a_j x_{ij} \tag{3}$$

where a_0 and a_j are, respectively, the intercept term and linear coefficient for the jth predictor variable. The method has been more refined by Hastie and Tibshirani (1986) so that the linear terms are replaced by arbitrary mathematical functions $f_j(.)$:

$$\frac{e^{p_i}}{1+e^{p_i}} = a_0 + \sum_{j=1,m} f_j(x_{ij}) \tag{4}$$

These functions are estimated using nonparametric techniques outlined in the paper mentioned above. It is this methodology that we adopt, since it affords greater flexibility in modelling the relationship between Dmin and sensitivity.

Table 4. Error sources in LOS.

In order to investigate the effect of the two predictors (i.e. Dmin and sensitivity) on the probability, we assign these two variables as predictors in equation (4). The statistical modelling is conducted in the statistical package R which provides a variety of statistical and graphical techniques (R Development Core Team 2005). The relationship between each predictor variable and the predicted probability may be visualized by setting the other predictor to the mean value, and graphing the functional relationship between probability and the predictor under scrutiny. The results of this procedure are plotted in figures 17 and 18.

As shown in figure 17, the probability of an incorrect prediction decreases as Dmin increases. In figure 18, the probability increases steadily as the sensitivity gets higher. Recall that only satellites modelled as visible by the surface model are considered in the experiment, and consequently the probability of an incorrect prediction can be used to calculate the probability of at least four satellites visible (i.e. $P(S)$) as follows:

$$P(S) = \prod_{i=1}^{4} (1 - P(S_i)) \tag{5}$$

The logistic regression model shown in figure 17 can then be used to predict $P(S_i)$ for each of the satellites modelled visible with a range of Dmin values that are computed from each pixel cell centre of the raster digital surface model. In addition, as there may be more than four satellites visible to a particular location, all the visible satellites are sorted according to Dmin values in descending order prior to the probability calculation (i.e. four satellites with larger Dmin values are chosen to provide the most reliable probability). Figure 19 shows the resulting probable viewshed created using nearest neighbour interpolation.

It is very interesting that the probable viewshed resembles the actual digital surface model, as the probability of at least four satellites visible is higher on the

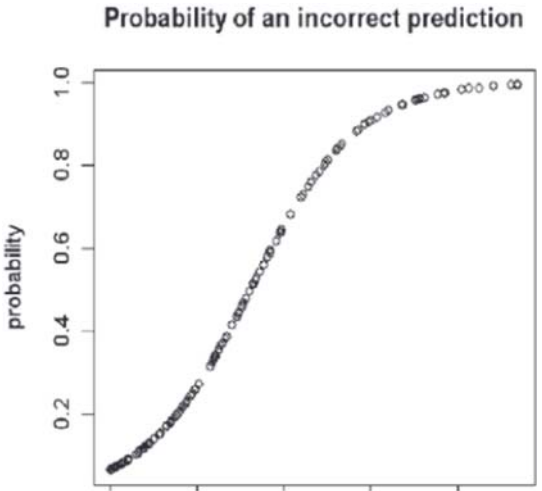

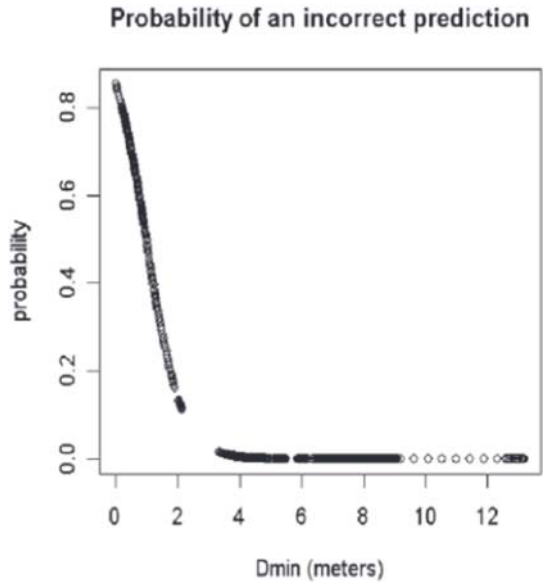

Figure 18. Probability vs sensitivity.

roof and open areas, and lower in the areas near buildings. Building outlines can still be clearly seen on this raster image although the pixel value is the probability instead of the height in metres. This raster image proves that the chosen regression model is appropriate.

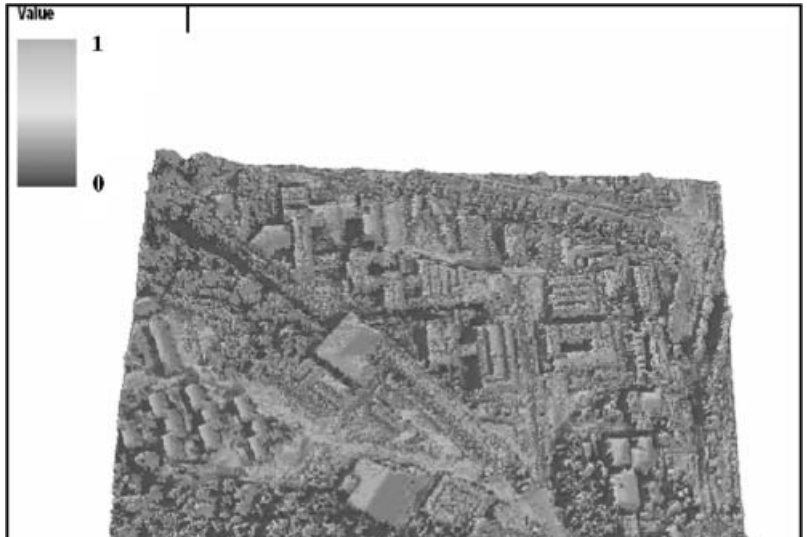

8. Conclusion

The real-time simulation and modelling of GPS availability has been conducted in a densely built-up area. The initial testing results have been presented. The newly developed mission planning software tool has implemented a variety of techniques including LOS scaling, coordinate transformation, and LOS analysis, and is capable of working with various forms of digital surface models (e.g. vector, raster and TIN). It has been proven that LiDAR is the most appropriate data set for modelling and predicting GPS satellites' availability in terms of reliability, productivity and accuracy.

Future work will focus on predicting GPS multipath effects in different terrain environments.

Acknowledgements

The authors express thanks to the Ordnance Survey for providing OS Master Map data and InfoTerra for the LiDAR data used in this work.

References

Boulianne, M., Santerre, R., Gagnon, P. and Nolette, C., 1996, Floating lines and cones for use as a GPS mission planning aid. *Photogrammetric Engineering & Remote Sensing*, **62**(3), pp. 311–315.

Chambers, J.M. and Hastie, T.J., 1992, *Statistical Models in S* (London: Chapman & Hall).

Dorey, M., 2002, Digital elevation models for intervisibility analysis and visual impact. PhD thesis, University of Glamorgan, Pontypridd, Wales, UK.

Gentle, J.E., 2003, *Random Number Generation and Monte Carlo Methods* (New York: Springer).

Hastie, T. and Tibshirani, R., 1986, Generalised additive models. *Statistical Science*, **1**(3), pp. 297–318.

Hosmer, D.W. and Lemeshow, S., 1989, *Applied Logistic Regression* (New York: John Wiley & Sons).

Jones, C., 1997, *Geographical Information Systems and Computer Cartography* (Boston, MA: Addison-Wesley).

Kidner, D.B., 2003, Higher order interpolation of regular grid digital elevation models. *International Journal of Remote Sensing*, **24**(14), pp. 2981–2987.

Ordnance Survey, 2004, A guide to Coordinate Systems in Great Britain. Available online at: http://www.gps.gov.uk/guidecontents.asp (accessed 23 February 2005).

Ordnance Survey, 2005, OS MasterMap user guide. Available online at: http://www.ordnancesurvey.co.uk/oswebsite/products/osmastermap/guides/userguide.html (accessed 12 January 2006).

Parsons, J.D., 2000, *The Mobile Radio Propagation Channel*, pp. 36–37 (Chichester: Wiley).

R Development Core Team, 2005, R: A language and environment for statistical computing, Vienna, Austria. Available online at: http://www.r-project.org/ (accessed 26 October 2005).

Thompson, G.F. and Manue, D.F., 2001, Issues and answers in quality control of LiDAR DEMs, LiDAR quality control report, pp. 119–122. Available online at: http://www.ncfloodmaps.com/pubdocs (accessed 14 August 2006).

Tse, R. and Gold, C., 2003, A proposed connectivity-based model for a 3D cadastre

VRHOVSKI, D., 2003, Satellite visibility in simulating urban satellite positioning-based road user charging. In *Proceedings of ION GPS/GNSS 2003*, Portland, Oregon, USA.

WALKER, R. and SANG, J., 1997, Mission planning for high precision RTK GPS surveying using accurate digital terrain information. In *Proceedings of ION GPS 1997 Conference*, Kansas City, Missouri, USA.